Electronic Supplementary Material (ESI) for Physical Chemistry Chemical Physics.

Supplementary Information

About the electronic and photophysical properties of Iridium (III)-pyrazino[2,3-f][1,10]-phenanthroline based complexes to use in electroluminescent devices

Diego Cortés-Arriagada[a,*], *Luis Sanhueza*[b,*], *Iván González*[c], *Paulina Dreyse*[d] *and Alejandro Toro-Labbé*[a]

[a]*Nucleus Millennium Chemical Processes and Catalysis; Laboratorio de Química Teórica Computacional (QTC), Facultad de Química, Pontificia Universidad Católica de Chile, Av. Vicuña Mackenna 4860, Macul, Santiago, Chile. *Email: dcortesr@uc.cl*

[b]*Instituto de Ciencias Químicas, Facultad de Ciencias, Universidad Austral de Chile, Casilla 567, Valdivia, Chile*

[c]*Departamento de Química Inorgánica. Pontificia Universidad Católica de Chile, Av. Vicuña Mackenna 4860, Macul, Santiago, Chile. Vicuña Mackenna 4860, Macul, Santiago, Chile.*

[d]*Departamento de Química, Universidad Técnica Federico Santa María, Av. España 1680, Valparaíso, Chile.*

S1. Geometries of the ground state S_0 and the first triplet state T_1

Selected geometrical parameters for the nine structures studied, including the $S_0$and T_1 states, are listed in Table S1. The general sketch labeling of the atoms, for the selected parameters, is presented in Figure S1. The complexes match with the C_2v symmetry. The N_1 and N_2 atoms of the C^N ligands are located in *trans* position, in agreement with the reported characterizations for another cyclometalated-Ir^{III} complexes.

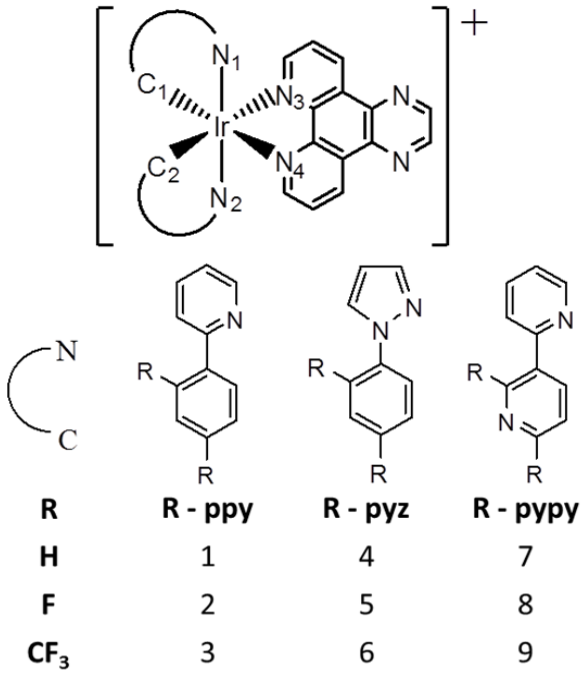

R	R - ppy	R - pyz	R - pypy
H	1	4	7
F	2	5	8
CF_3	3	6	9

Fig. S1 Sketch labeling for the nine systems studied.

Table S1. Selected bond lengths (Å) and angles (°) for the S_0 and T_1 states of complexes **1**-**9**.

S_0	1	2	3	4	5	6	7	8	9
distances									
*r*Ir - C1	2,021	2,019	2,016	2,031	2,030	2,025	2,015	2,013	2,010
*r*Ir - N1	2,084	2,083	2,073	2,055	2,055	2,042	2,088	2,087	2,078
*r*Ir - N3	2,226	2,219	2,228	2,214	2,206	2,212	2,223	2,216	2,224
angles									
∠C1 - Ir - N1	80,1	80,1	79,3	79,6	79,8	78,8	80,1	80,2	79,5
∠N3 - Ir - N4	75,2	75,5	75,2	75,7	76,0	75,8	75,3	75,6	75,3
∠N1 - Ir - N2	173,4	173,4	173,0	172,5	172,6	172,6	173,2	173,3	172,8
∠C1 - Ir - N4	172,2	172,6	171,9	172,1	172,4	172,1	172,3	172,7	172,1
dihedrals									
∠N1-C1-N2-N4	8,8	8,6	9,4	8,7	8,4	8,5	8,8	8,5	9,4
∠C1-C2-N4-N3	3,7	3,4	3,1	6,0	5,9	6,0	3,8	3,6	3,1
∠C2-N2-N3-N1	8,3	8,1	8,8	8,3	8,0	8,2	8,2	8,0	8,8

T_1	1	2	3	4	5	6	7	8	9
distances									
*r*Ir - C1	1,991	1,992	1,988	1,998	2,001	1,995	1,994	2,003	1,999
*r*Ir - N1	2,079	2,078	2,067	2,049	2,049	2,038	2,083	2,075	2,069
*r*Ir - N3	2,222	2,210	2,215	2,206	2,193	2,199	2,212	2,192	2,195
angles									
∠C1 - Ir - N1	80,9	81,0	80,0	80,3	80,5	79,5	81,0	80,9	79,9
∠N3 - Ir - N4	75,7	76,1	75,9	76,2	76,6	76,3	75,9	76,8	76,8
∠N1 - Ir - N2	177,2	177,0	176,4	176,2	176,2	176,4	177,0	176,2	175,7
∠C1 - Ir - N4	169,7	170,3	170,0	169,1	169,8	168,9	169,9	172,6	172,3
dihedrals									
∠N1-C1-N2-N4	8,7	8,4	9,0	8,9	8,4	8,9	8,7	7,0	7,6
∠C1-C2-N4-N3	4,6	4,2	4,2	7,3	7,2	7,7	4,0	3,7	3,7
∠C2-N2-N3-N1	8,3	8,1	8,6	8,7	8,2	8,6	8,4	6,8	7,2

The first triplet state T_1 for all systems was also studied. In this case the bond lengths involving the Ir-C^N ligand have a similar behavior when H is replaced by F or CF_3 group with a same tendency to the shorter distances and angle values due to the presence of fluorinated substituents in the three series is assumed (**1**-**3**,**4**-**6** and **7**-**9**). On the other hand,

the distances involved in the Ir-C^N ligand and the Ir-N^N ligand, are contracted when are compared to their respective S_0 state. In addition to these shorter bonds, the angle values concerning the metal center and the same ligand (∠C1-Ir-N1 and ∠N3-Ir-N4) are in general longer in the T_1 state, compared to their respective S_0 state. As can also be observed by other authors, a contracted length in T_1 state, compared to the S_0 state can be assumed as an indication of the participation of the respective C^N ligand on the frontier molecular orbitals, in both, the ground and the excited state, and inducing different electronic transitions and/or contributions to the absorption spectra in complexes[1, 2].

S2. Orbital composition analysis

Table S2. Fragment contributions to HOMO and LUMO; orbital composition analysis was computed according to the Ros-Schuit partition scheme in the Multiwfn code[3].

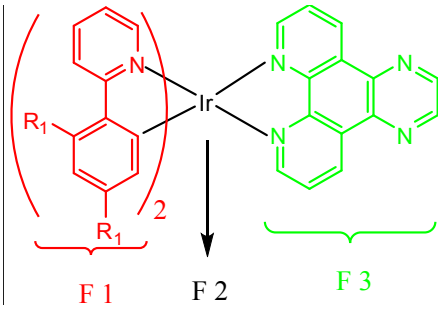

system	HOMO			LUMO		
	F1	F2	F3	F1	F2	F3
1	51,51	44,36	4,12	1,61	2,62	95,77
2	54,76	41,76	3,48	1,75	2,92	95,34
3	49,27	47,47	3,27	2,30	2,89	94,82
4	55,38	40,79	3,83	1,27	2,83	95,91
5	64,05	33,13	2,82	1,38	3,11	95,51
6	53,02	43,60	3,38	1,54	3,18	95,28
7	46,49	50,38	3,13	1,59	2,00	96,41
8	55,64	42,21	2,15	1,73	2,36	95,91
9	44,57	52,75	2,69	6,44	2,20	91,36

S3. Extra data for singlet-singlet allowed transitions

Table S3. Data for low-lying singlet excited states of complexes **1-9** computed in CH_2Cl_2. Absorption wavelength (λ_{max}), oscillator strength, monoexcitations (and coefficient of the excited state wavefunction), and description of the electron transition. C^N, H and L stand for the ciclometalating ligand, HOMO and LUMO, respectively.

system	λ_{max} (nm)	*f*	monoexcitations	description
1	383	0.039	H-1->L (0.46)	Ir(d)+C^N(π)→ppl(π*); MLCT/LLCT
	361	0.061	H-3->L (0.60)	Ir(d)→ppl(π*); MLCT
2	373	0.040	H-1->L (0.65)	Ir(d)+C^N(π)→ppl(π*); MLCT/LLCT
	348	0.086	H-4->L (0.60)	Ir(d)→ppl(π*); MLCT
3	352	0.152	H-2->L (0.62)	Ir(d)+C^N(π)→ppl(π*); MLCT/LLCT
4	373	0.099	H-3->L (0.65)	Ir(d)+C^N(π)→ppl(π*); MLCT/LLCT
	349	0.024	H-2->L+2 (0.67)	Ir(d)+C^N(π)→ppl(π*); MLCT/LLCT
5	359	0.108	H-4->L (0.67)	Ir(d)+C^N(π)→ppl(π*); MLCT/LLCT
6	356	0.116	H-2->L (0.67)	Ir(d)+C^N(π)→ppl(π*); MLCT/LLCT
7	361	0.103	H-1->L (0.61)	Ir(d)+C^N(π)→ppl(π*); MLCT/LLCT
8	354	0.063	H-1->L (0.64)	Ir(d)+C^N(π)→ppl(π*); MLCT/LLCT
9	342	0.063	H-1->L (0.49)	Ir(d)+C^N(π)→ppl(π*); MLCT/LLCT
			H->L+4 (0.39)	Ir(d)+C^N(π)→ppl(π*); MLCT/LLCT

S4. Spin density distribution onto the first triplet excited states (T_1)

Firstly, the TD-DFT gradients were used to obtain the first triplet excited states; this method allows to account for the correct molecular orbital pairs contributing to the excited state wavefunction and converges to the optimized state by using a restricted wavefunction,

which is not possible (although approximate) by adopting a ground state geometry optimization at the unrestricted level (this is in a triplet state where a electron is promoted from an occupied to an unoccupied molecular orbital in the unrestricted formalism by using a single-orbital pair model). The latter turns possible when the excited state shows a low multiconfigurational character (for instance, the transition is only due to HOMO→LUMO electron promotion), but some of the presented complexes show multiconfigurational triplet states as will be shown later. For subsequent analysis, the total energy of the T_1 state was obtained in an unrestricted formalism, and we check the wavefunction consistency by analyzing the spin density distribution in comparison with the results from TD-DFT calculations. Condensed spin density values are depicted in Table S4, and spin density surfaces are displayed in Figure S2. In the triplet state, two unpaired electrons are delocalized around all the complexes and its topology must to be in accord with the hole-electron distribution in Figure 4 (in the main article) to account for the correct electronic description. From Table S4, it is observed that for complexes **1**-**7**, we found that one unpaired electron is delocalized in the metal center (~0.5|*e*|) and the C^N ligands (~0.5|*e*|), while the remaining unpaired electron is delocalized in the N^N ligand; these results are consistent with the hole-electron distributions (Figure 4 in the main article) and they indicate that these states are deactivated by electron transfer from the ancillary ligand (where the LUMO is located) until the metal and C^N ligands (where the HOMO resides). Furthermore, we found that the unpaired electrons of the N^N ligand increases from ~1.0|*e*| to 1.25|*e*| and 1.26|*e*| in complexes **8** and **9**, respectively, in agreement with the increased ^{3}LC character (and decreased ^{3}LLCT) of the T_1 state in these systems as observed from the TD-DFT results (Table 1 in the main article); thus, the deactivation of the emissive state in

complexes **8-9** occurs by electron transfer from the ancillary ligand until the metal and cyclometallated ligands, in addition to the ligand centered charge transfer in the ancillary ligand.

Table S4. Condensed electron spin density for the complexes **1-9** corresponding to the optimized T_1 states.

system	ρ_s(Ir)	ρ_s(C^N)	ρ_s(N^N)
1	0.49	0.49	1.02
2	0.50	0.49	1.02
3	0.53	0.46	1.00
4	0.44	0.54	1.02
5	0.42	0.56	1.02
6	0.47	0.51	1.03
7	0.55	0.42	1.03
8	0.49	0.26	1.25
9	0.46	0.18	1.36

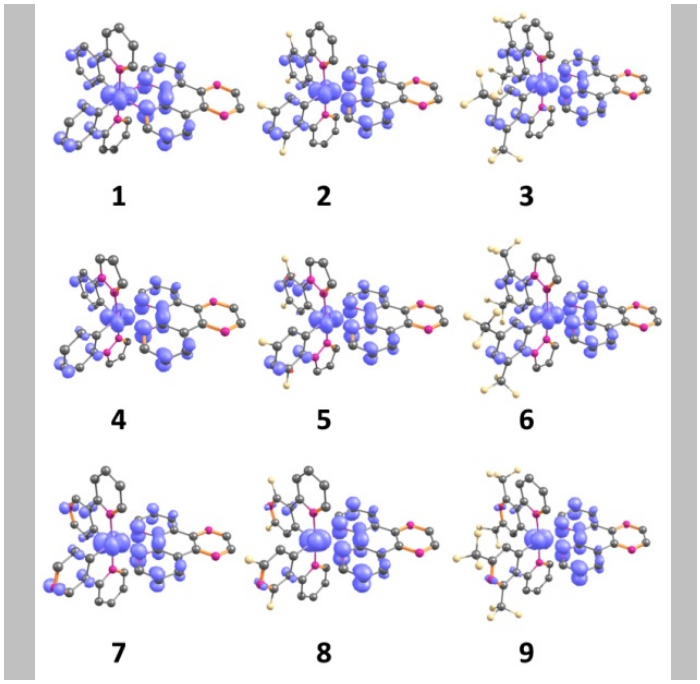

Fig. S2 Electron spin density for the complexes **1-9** corresponding to the optimized T_1 states.

S5. Geometrical parameters of metal-centered triplet excited states

Table S5. Selected geometrical parameters of metal-centered triplet excited states (^{3}MC) of complexes **1-9**. The atom labels are depicted in Figure S1.

Parameter	***Complex***								
	1	**2**	**3**	**4**	**5**	**6**	**7**	**8**	**9**
distances									
*r*Ir - C1	2,027	2,031	2,031	2,003	2,006	2,04	2,021	2,032	2,033
*r*Ir - N1	2,580	2,561	2,546	2,527	2,505	2,569	2,500	2,469	2,455
*r*Ir - C2	2,028	2,031	2,031	2,003	2,006	2,035	2,021	2,032	2,034
*r*Ir - N2	2,298	2.260	2,265	2,526	2,505	2,197	2,500	2,470	2,448
*r*Ir - N3	2,249	2,235	2,234	2,226	2,218	2,228	2,227	2,212	2,216
*r*Ir - N4	2,285	2,294	2,266	2,227	2,218	2,268	2,227	2,212	2,217
angles									
∠C1 - Ir - N1	72,1	71,9	71,85	75,0	75,1	71,1	74,9	74,7	74,5
∠C2 - Ir - N2	77,7	77,8	77,26	75,0	75,2	77,3	74,9	74,7	74,6
∠N3 - Ir - N4	73,4	73,7	74,1	74,4	74,7	74,4	75,2	75,9	75,8
∠N1 - Ir - N2	155,7	154,9	159,5	170,3	170,0	158,5	172,7	173,0	172,3
∠C1 - Ir - N4	147,4	147,6	150,0	169,2	169,7	144,8	172,8	173,6	173,0
∠C2 - Ir - N3	175,4	175,7	174,8	169,1	169,6	175,2	172,8	173,6	173,2
dihedrals									
∠N1-C1-N2-N4	17,6	16,8	16,1	13,5	13,2	14,4	9,4	7,5	8,4
∠C1-C2-N4-N3	21,2	21,2	19,7	3,2	3,3	23,7	1,6	5,0	5,1
∠C2-N2-N3-N1	15,4	15,9	11,2	12,0	11,7	13,1	8,5	6,9	7,6

S7. Benchmark with other DFT functionals

To test the reliability of the selected methodology, we perform a benchmark study with the B3LYP[4], CAM-B3LYP[5], TPSSh[6], and BHandHLYP[7] functionals, and we compare with the experimental absorption/emission energies of the complex **1** (Table S6)[8]. The used basis set and pseudopotential is the same for all the methodologies as described in the manuscript.

Table S6. Absorption wavelength of the low-lying singlet excited states and emission wavelenghts from T1 state for the complex **1** (computed in CH_2Cl_2 as solvent).

Functional	λabs (nm)		λemi (nm)
B3LYP	383	361	597
CAM-B3LYP	335	329	550
BHandHLYP	316	-	542
TPSSH	444	416	619
Experimental[8]	382	358	590

We observe that the B3LYP functional has the best performance to describe the absorption/emission energies, while the rest of the methods show higher deviations with respect to the experimental measure in CH_2Cl_2. Clearly, the TPSSh functional overestimates the absorption wavelengths due to ^{1}MLCT/LLCT transitions, and then the emission is computed red-shifted in comparison with the experimental measure. On the

other side, the CAM-B3LYP and BHandHLYP methods underestimate the absorption/emission wavelengths and these appear extremely blue-shifted in comparison with the experimental result. Therefore, the B3LYP functional performs as the best method to description of photophysical properties of complex **1**. In this regard, although the DFT methodologies are known to be difficult to describe charge-transfer states, all the works comparing experimental and theoretical properties of Ir (III) complexes, indicate that the percentage of exact exchange in the B3LYP functional is adequate for a description of these states in the mentioned systems. In this framework, the CAM-B3LYP functional would be a preferable DFT functional to study the charge-transfer states due to its long-range corrected nature; however, we clearly observe that CAM-B3LYP overestimates the absorption/emission energies from the benchmark (at least in 47 nm in comparison with respect to the B3LYP results). In addition, the B3LYP functional is recommended in a recent protocol to obtain accurate photophysical parameters of Ir(III) complexes, such as emission energies, and radiative rates[9].

S7. References

1. Y. You and S. Y. Park, Dalton Transactions, 2009, 1267-1282.
2. Y. You and W. Nam, Chemical Society Reviews, 2012, 41, 7061-7084.
3. T. Lu and F. Chen, Journal of Computational Chemistry, 2012, 33, 580-592.
4. A. D. Becke, The Journal of Chemical Physics, 1993, 98, 5648-5652.
5. T. Yanai, D. P. Tew and N. C. Handy, Chemical Physics Letters, 2004, 393, 51-57.
6. J. Tao, J. P. Perdew, V. N. Staroverov and G. E. Scuseria, Physical Review Letters, 2003, 91, 146401.

7. A. D. Becke, The Journal of Chemical Physics, 1993, 98, 1372-1377.

8. K. K. W. Lo, C. K. Chung and N. Zhu, Chemistry-a European Journal, 2006, 12, 1500-1512.

9. J. M. Younker and K. D. Dobbs, The Journal of Physical Chemistry C, 2013, 117, 25714-25723.